Experimental and Analytical Study of Cracks under Biaxial Fatigue

M. Mokhtarishirazbad[1], P. Lopez-Crespo[1], B. Moreno[1], D. Camas[1], A. Lopez-Moreno[2], M. Zanganeh[3]

[1] Department of Civil and Materials Engineering, University of Malaga, C/Dr Ortiz Ramos s/n, 29071, Malaga, Spain, plopezcrespo@uma.es
[2] Department of Materials Science and Metallurgy Engineering, University of Jaen, Campus Las Lagunillas, 23071, Jaen, Spain, alopez@ujaen.es
[3] *ORAU, Oak Ridge, TN, USA*, Houston TX, USA
mohammad.zanganehgheshlaghi@nasa.gov

ABSTRACT. *Most mechanical components experience multi-axial cyclic loading conditions during service. Experimental analysis of fatigue cracks under such conditions is not easy and most works tend to focus more on the simpler but less realistic case of uni-axial loading. Consequently, there are many uncertainties related to the load sequence effect that are now well known and are not normally incorporated into the growth models. The current work presents a new methodology for evaluating overload effect in biaxial fatigue cracks. The methodology includes evaluation of mixed-mode (KI and KII) stress intensity factor and the Crack Opening Displacement for samples with and without overload cycle under biaxial loading. The methodology is tested under a range of crack lengths. All crack-tip information is obtained with a hybrid methodology that combines experimental full-field digital image correlation data and Williams' elastic model describing the crack-tip field.*

INTRODUCTION

Reliable life-time prediction of structural materials subjected to external loadings depends strongly on the accuracy of the fracture parameters estimation. So far, a number of successful approaches have been presented for estimating the essential fracture parameters such as stress intensity factors (SIFs) experimentally [1]. Apart from the conventional standard test methods [2], it has been shown that crack-tip fields (strain, stress and displacement field) include essential information for accurate estimation of fracture parameters [3]. A number of different techniques are able to provide both surface and bulk information. Surface techniques include photo-elasticity [4], thermo-elasticity [5], Moiré interferometry [6] and digital image correlation (DIC) [7]. Bulk techniques include neutron diffraction [8] and X-ray diffraction [9]. Among all these full-field techniques, DIC has received enormous attention recently [10,11] because of its many advantages compared to other techniques [12]. Simplicity, accuracy and flexibility are the most prominent merits of DIC technique for calculating

displacement fields [13]. While fracture problems can be simplified by considering mode I loading, cracks in structural materials are generally under mixed-mode loading condition [3]. Therefore, estimation of the fracture parameters based on mixed-mode loading condition will be more representative of the material fracture behaviour under the actual working condition. Different optical methods have been used for obtaining full-field information required for mixed-mode loading analysis previously. Sanford and Dally [14] have determined the mixed-mode SIFs by utilizing isochromatic fringes near the crack-tip. They have reported that employing an over-deterministic approach on the data points provided by the full filed fringe patterns led to a highly accurate SIF estimation. Displacement fields derived by DIC technique has been utilized by Yoneyama et al. [15] to evaluate the mixed-mode SIFs of a polymer (polymethylmethactylate). While they used a non-linear least square method for their solutions, Réthoré et al. has develop a method based on the Lagrangian conservation law for mixed-mode SIFs estimations. A good agreement between analytical displacement fields generated based on the Muskhilishvili's complex function approach and the experimentally measured displacement fields (obtained by DIC) has been also reported by Lopez-Crespo et al [16]. By fitting nominal and experimental data, they have determined mixed-mode SIFs for a crack in a fastener hole. For estimating the crack closure level by DIC, virtual extensometers can be introduced behind the crack-tip for local measurements of crack opening displacement. Nowell et al. [6] have compared Moiré interferometry techniques with DIC method for studying closure levels of propagating fatigue cracks. The effect of overloads on the crack growth has been studied under uniaxial loads with a number of different experimental techniques. These include photo-elasticity [17], pulse reflection microscope [18], electronic speckle pattern interferometry [19] and synchrotron X-ray diffraction [20,21]. However, the overload effect under biaxial conditions is much less studied.

In the present paper, we use a hybrid method for estimating mixed-mode SIF from in-plane crack-tip displacements obtained by DIC. This is used for studying the effect of overload under biaxial loading. The methodology can be used to evaluate crack closure level before and after applying the overload cycle from local crack opening displacement.

MATERIALS AND METHODS

Crack propagation in a low carbon steel (St-52-3N) was studied [22]. Table 1 shows the composition of the alloy. Microstructural examination with the optical microscope has revealed ferrite and pearlite bands as vertical black and white bands respectively [23]. A schematic of the geometry is shown in Fig. 1.

Table 2. Chemical composition in weight % of St-52-3N steel. The balance is Fe.

C	Si	Mn	P	S	Cr	Ni	Mo
0.17	0.22	1.23	0.01	>0.0001	0.07	0.06	0.16

Table 2. Monotonic properties of St-52-3N steel.

Yield stress, σ_y	386 MPa
Ultimate tensile stress, σ_u	639 MPa
Young's modulus, E	206 GPa
Shear Modulus	78 GPa

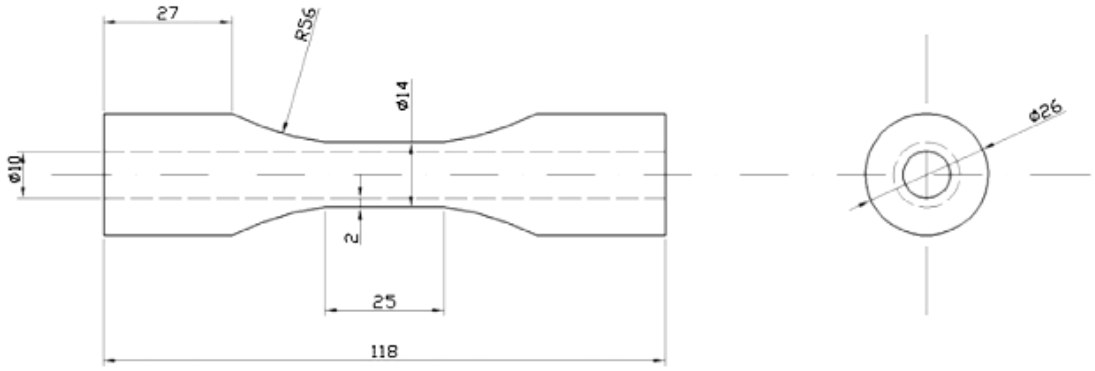

Figure 1. Geometry of the tubular dog-bone specimen with central hole. All dimensions are in mm.

A MTS 809 servo-hydraulic loading rig coupled by a biaxial extensometer Epsilon 3550 was used to apply biaxial loads under stress control mode in a similar way to previous works [22,24]. Cyclic sinus signal with axial load ratio of 0.1 (R_a = 0.1) and torsional load ratio of -1 (R_t=-1) was applied while the angle between the axial and the torsional stress, φ, was set to 45°. Fig. 2 shows how φ has been defined. In order to study the effect of the overload on the crack propagation behaviour, a 40% overload was applied when the crack length for the specimen S2 was 0.669 mm. That is, the load range in the overload cycle was 1.4 times larger than load range during the rest of the test. The cyclic loading then continued until the crack length reached 1.4 mm. Table 3 shows the loading condition of for samples with and without overload.

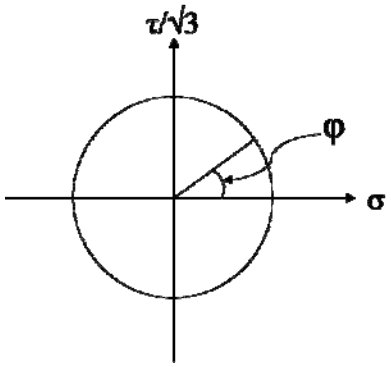

Figure 2. Definition of axial and shear stress amplitude.

Table 3. Axial and shear stress values for specimens with and without overload cycle.

Specimen	Hole diameter (mm)	Cross section area (mm^2)	σ_{max}	τ_{max}	σ_{OL}	τ_{OL}
S1	0.333	73.4	240	138.5	-	-
S2	0.336	74.8	240	138.5	336	194

In addition, to evaluate the closure level, near tip crack opening displacement were measured by DIC [25,26]. In this regard, a virtual extensometer was appointed to measure the displacement in the crack opening direction with distances in the range of 20 to 200 μm with the interval of 20 μm behind the crack-tip. Fig 3, shows an example of the positions of the virtual extensometer.

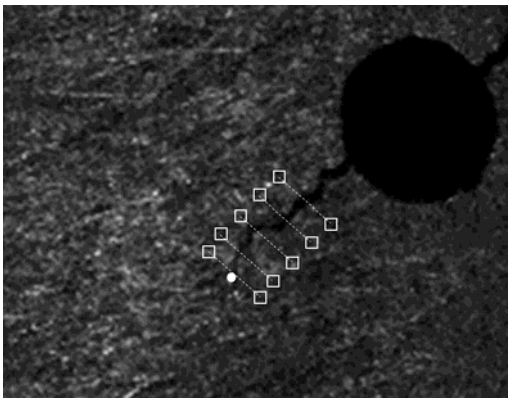

Figure 3. The position of virtual extensometers for COD examination. The white bold mark shows the crack-tip position.

FATIGUE CRACK GROWTH

Fig. 4 shows how applying overload can affect the crack growth behaviour. The retardation in the crack growth after applying an overload cycle can be seen in this graph. The general regimes of crack growth rate after overload are acceleration, retardation and recovery [27]. Acceleration in crack growth rate immediate after overload has been attributed to the crack tip stretching which can lead to increasing the effective stress intensity range [27]. However, 5 cycles after the overload we did not observe such acceleration in the crack growth rate (Fig. 5). One possible reason could be the fracture of the stretched crack ligament during the overload cycle [27]. There was a retardation period in the crack growth after the overload cycle of 8000 cycles, thus increasing the total life by ~14%. Crack closure is one of the mechanisms for explaining this retardation [27,28]. The crack was extended by almost 40 μm over 2300 cycles, during this period. Retardation period usually takes hundreds of cycles, while recovery step occurs over thousands of cycles.

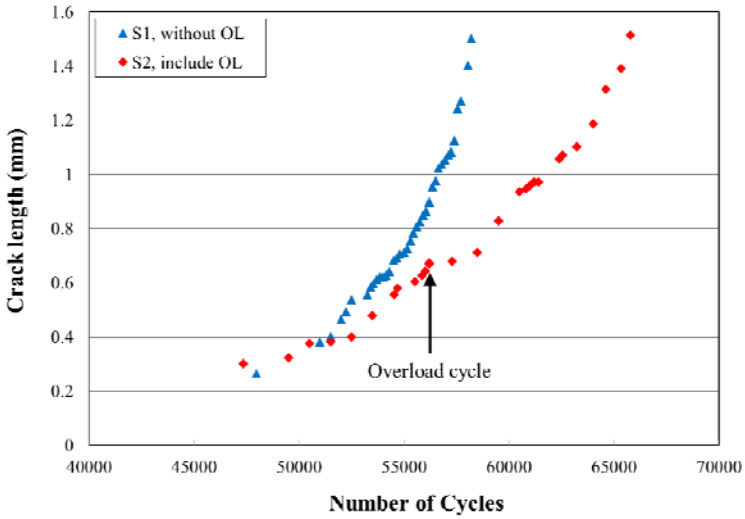

Figure 4. Evolution of crack length by number of cycles for samples with and without overload cycle.

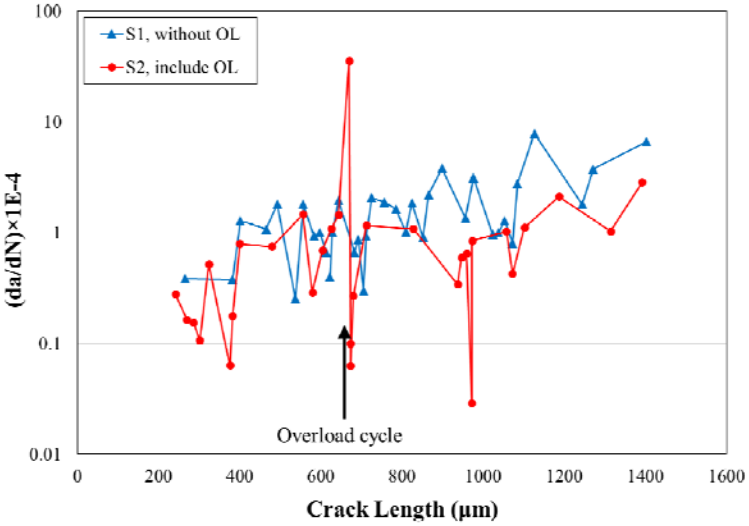

Figure 5. Crack growth rate in logarithmic scale as a function of the crack length for both samples S1 and S2. The black arrow shows where the overload cycle has been applied.

PROCESSING OF DISPLACEMENT INFORMATION

Displacement data ahead of the crack was measured by using DIC. The obtained displacement data was then fitted into Williams' series [29,30]:

$$Mode I \begin{cases} u_I = \sum_{n=1}^{\infty} \frac{r^{\frac{n}{2}}}{2\mu} a_n \left\{ \left[\kappa + \frac{n}{2} + (-1)^n \right] \cos\frac{n\theta}{2} - \frac{n}{2}\cos\frac{(n-4)\theta}{2} \right\} \\ v_I = \sum_{n=1}^{\infty} \frac{r^{\frac{n}{2}}}{2\mu} a_n \left\{ \left[\kappa - \frac{n}{2} - (-1)^n \right] \sin\frac{n\theta}{2} + \frac{n}{2}\sin\frac{(n-4)\theta}{2} \right\} \end{cases} \quad (1)$$

and

$$Mode II \begin{cases} u_{II} = -\sum_{n=1}^{\infty} \frac{r^{\frac{n}{2}}}{2\mu} b_n \left\{ \left[\kappa + \frac{n}{2} - (-1)^n \right] \sin\frac{n\theta}{2} - \frac{n}{2}\sin\frac{(n-4)\theta}{2} \right\} \\ v_{II} = \sum_{n=1}^{\infty} \frac{r^{\frac{n}{2}}}{2\mu} b_n \left\{ \left[\kappa - \frac{n}{2} + (-1)^n \right] \cos\frac{n\theta}{2} + \frac{n}{2}\cos\frac{(n-4)\theta}{2} \right\} \end{cases} \quad (2)$$

where u_I and v_I are horizontal and vertical displacements in mode I respectively, u_{II} and v_{II} are horizontal and vertical displacements in mode II respectively, μ is the shear modulus, $\kappa = (3-\nu)/(1+\nu)$ for plane stress and $\kappa = 3-4\nu$ for plane strain condition, υ is the Poisson's ratio, r and θ are polar coordinates with the crack-tip being the origin of coordinates, and a and b are constants.

Eqs. 1 and 2 can be written in terms of the SIFs and T-stress as follows:

$$u = \frac{K_I}{2\mu}\sqrt{\frac{r}{2\pi}}\cos\frac{\theta}{2}(\kappa - 1 + 2\sin^2\frac{\theta}{2}) + \frac{K_{II}}{2\mu}\sqrt{\frac{r}{2\pi}}\sin\frac{\theta}{2}(\kappa + 1 + 2\cos^2\frac{\theta}{2}) + \frac{T}{8\mu}r(\kappa+1)\cos\theta \quad (3)$$

$$v = \frac{K_I}{2\mu}\sqrt{\frac{r}{2\pi}}\sin\frac{\theta}{2}(\kappa + 1 - 2\cos^2\frac{\theta}{2}) - \frac{K_{II}}{2\mu}\sqrt{\frac{r}{2\pi}}\cos\frac{\theta}{2}(\kappa - 1 - 2\cos^2\frac{\theta}{2}) + \frac{T}{8\mu}r(\kappa-3)\sin\theta \quad (4)$$

by using

$$K_I = a_1\sqrt{2\pi}\,, \quad K_{II} = -b_1\sqrt{2\pi}\,, \quad T = 4a_2 \quad (5)$$

where K_I and K_{II} are mode I and II of SIF respectively and T represents T-stress.
Having employed a post processing routine, the crack opening displacement, COD, has been determined at various distances behind crack-tip. COD was determined as follows:

$$COD(x) = \sqrt{u_{bot}^2 + v_{bot}^2} - \sqrt{u_{top}^2 + v_{top}^2} \quad (6)$$

where u and v are the horizontal and vertical displacement respectively, and x is the distance of the extensometer behind the crack-tip. The subscripts "top" and "bot" refer to the position of the virtual extensometer points relative to the crack line.

RESULTS AND DISCUSSION

Fig. 6 shows how COD value changes by increasing the distance of the virtual extensometer from the crack-tip for crack lengths of 0.682 mm and 0.669 mm for sample S1 and S2 respectively. A similar trend has been previously observed [31]. The evolution of COD during a complete cycle (loading and unloading) at 60 µm behind the crack-tip for different crack lengths in samples S1 and S2 are shown in Fig. 7. The effect of applying an axial-torsional overload of 40% on the evolution of COD for sample S2 is clear in Fig. 7.b. While prior to the overload, COD at the maximum load was about 2 µm, just after overload, +5 cycles, the maximum COD reduced to about 1.2 µm. A return to the baseline closure load has been observed when the crack has progressed sufficiently beyond the overload event. It can be seen from Fig. 7.b that applying the overload reduces the COD by 49% with respect the sample S1 with no overload. This difference is more significant in Fig. 8b where the post overload situation is shown.

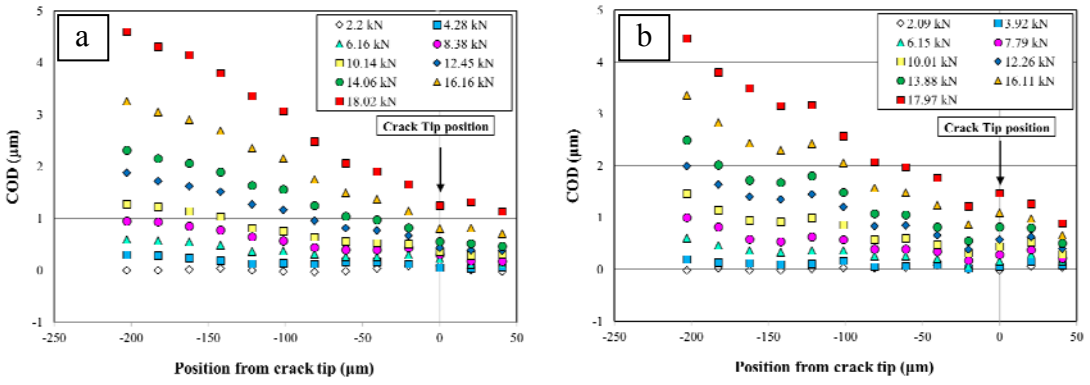

Figure 6. COD as a function of the position of the virtual extensometer with respect to the crack-tip for: a) sample S1 with a crack length of 0.682 mm after 69000 cycles and b) sample S2 with a crack length of 0.669 mm after 56190 cycles before overload.

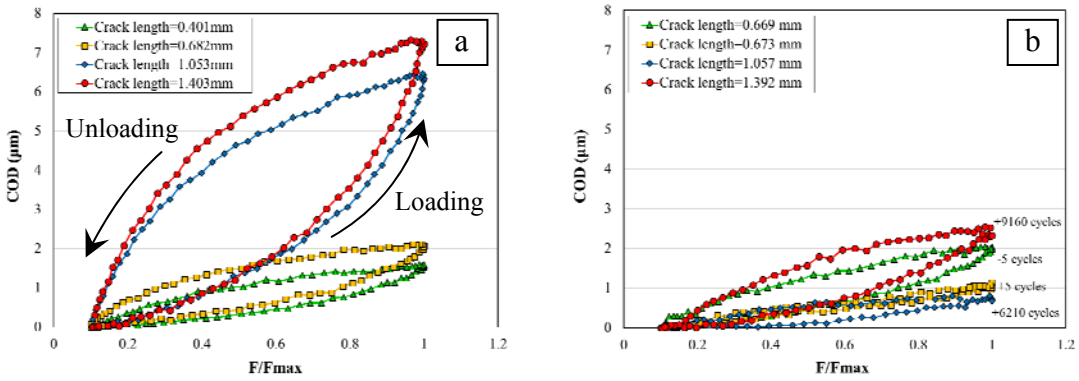

Figure 7. COD behaviour during loading and unloading cycle for different crack lengths for sample S1 and S2. The number of cycles before and after overload where overload cycle was considered as 0 cycle, are shown in the graph b.

A comparison between the COD behaviour in sample S1 and S2 in similar crack lengths was done at 60 µm behind the crack-tip and the results are shown in Fig. 8. Fig. 8.a shows the COD examination for a complete cycle for samples S1 and S2 with crack lengths of 0.669 mm and 0.682 mm respectively. The overload was not yet applied on S1 for the cycle described in Fig. 8.a. The similar COD curves for both samples can be attributed to similar crack length and loading condition for both samples. Fig. 8.b shows the evolution of a cycle in both samples once the overload has been applied to S2. The differences between S1 and S2 in Fig. 8.b are remarkable. IThe overload has a double influence on the COD: it decreases the overall COD value and also it modifies the shape of the COD curve (Fig. 8.b). This shape modification consists of the COD curve having a change in slope at a certain load (~0.2 F/Fmax). This change in slope is often referred as knee [32,33]. In Fig. 8.c-d show the loading and unloading parts of the cycle for both samples. The beginning and the end of the cycle appears magnified in Fig. 8.c-d. The influence of overload introducing this knee is particularly evident in the unloading part of the cycle (Fig. 8.d).

Displacement data ahead of the crack-tip then fitted to Williams' series in order to estimate the experimental SIFs and T-Stress values. In order to improve the quality of the SIF estimations, the recommendations given in [34] were followed. Accordingly, a high order interpolation scheme of optimized 8-tap spline was used for during DIC analysis to achieve sub-pixel accuracy. Zero-normalized sum of squared differences was set as the correlation criterion in order to vanish the effect of offset and scale in lighting [13]. The subset size was adjusted to 31×31 pixels. In addition, just 25% of the crack line was considered in the area of interest (the area where the displacement data were measured by DIC). By taking to account the size of the area of interest (0.4 ×0.4 mm2), two terms in the Williams' solution were used as suggested in [34]. In fact, neglecting T-stress which appears at the second term of Williams' series can also induce a significant error in SIFs calculations in short crack length examinations [3].

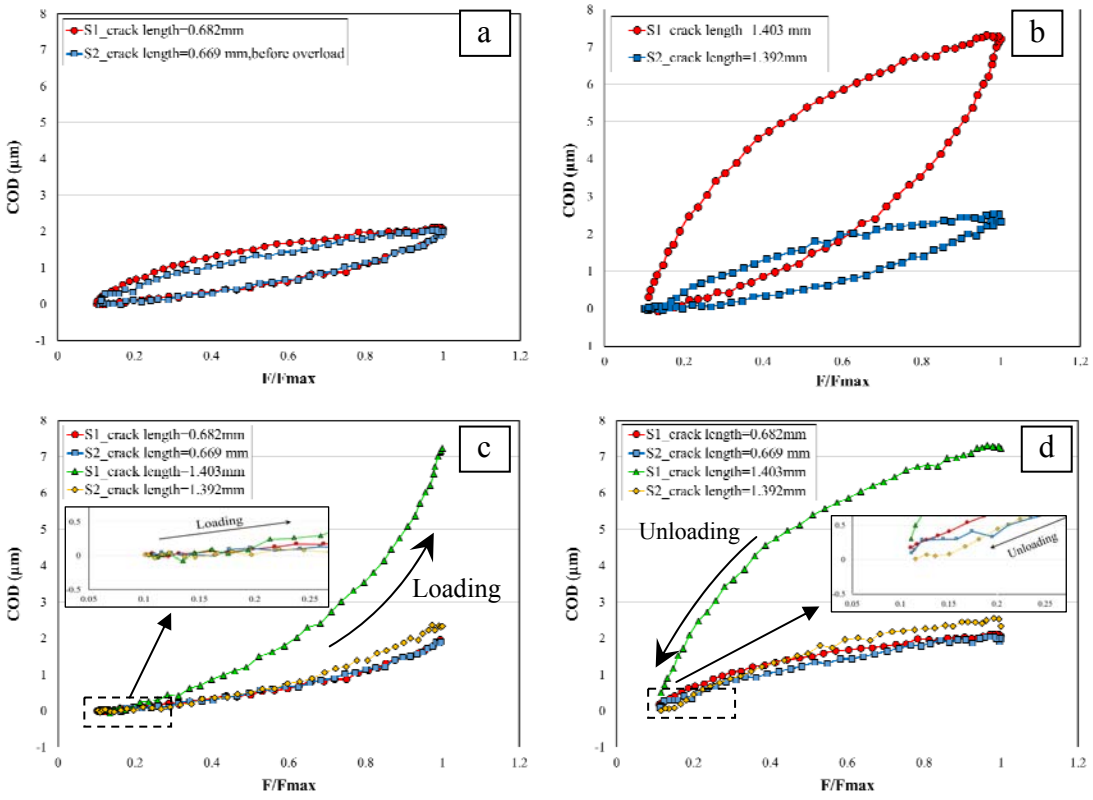

Figure 8. COD examination for different crack lengths of samples S1 and S2. a) COD for a crack length of 0.6 mm for both S1 and S2 before applying overload, b) difference between COD of samples S1 and S2 for crack length of 1.392 mm and 1.403 mm respectively, c) COD during the loading segment of a loading cycle, d) COD during unloading segment of a loading cycle.

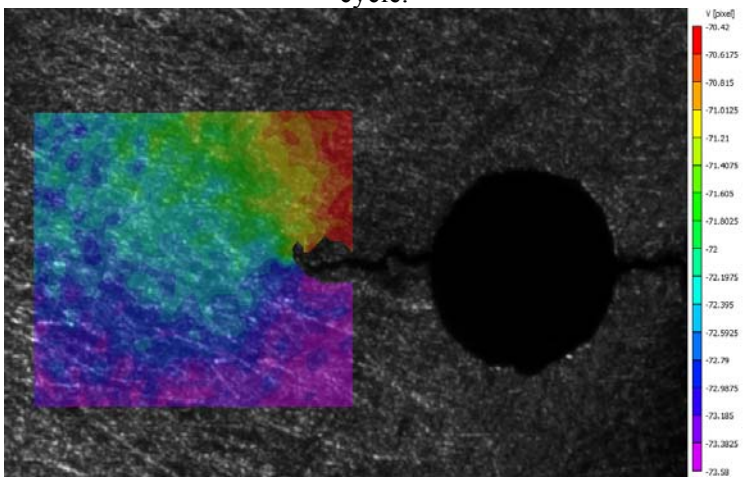

Figure 9. The position of the area of interest for deriving the displacement field ahead of a crack with the length of 0.479 mm after 53500 cycles (sample S2).

Table 4. The evaluation of SIFs and T-stress for two crack lengths in samples S1 and S2.

Specimen	Crack length (mm)	COD_{max} (μm)	ΔK_I (MPa√m)	ΔK_{II} (MPa√m)	T-stress (MPa√m)
S1	0.682	2.06	17.51	23.81	-669.94
S1	1.053	6.33	37.82	40.14	-1079.67
S2	0.669	1.98	13.19	23.16	-251.78
S2	1.057	0.71	9.67	23.56	-231.80

Fig. 9 illustrates the vertical displacement contour for an area of interest in front of a crack with a length of 0.479 mm of sample S2. Images were rotated 37° clockwise so that the crack line was horizontal [35].

Table 3 shows the results of SIF for different crack lengths. It can be seen that ΔK_I, ΔK_{II} and T-stress increase as the crack grows from 0.682 mm to 1.053 mm for sample S1. Table 4 also shows that applying an overload cycle in sample S2 decreases the SIFs even after propagating the crack by 0.388 mm. COD values in Table 4 indicate that the initial condition (crack length = 0.682 mm for S1 and crack length = 0.669 mm for S2) is equivalent for both samples. It can be seen that applying the overload drastically reduced the COD value. For the second crack length shown in Table 4, the COD raised to 6.33 μm in S1 and due to the overload effect, COD decreased to 0.71 μm. That is, the overload inverted the trend normally followed as the crack grows; for a similar baseline load, the COD increases as the crack grows. However, if an overload is applied, COD decreases as the crack grows, as long as the crack-tip is within the zone of influence of the overload.

The ΔK_I follows a similar trend to the COD. ΔK_I increases more than 200% for a 54% increment in the crack length in S1. However, ΔK_I decreases 27% for a 58% increment in the crack length in S2. With respect to ΔK_{II}, an increase of about 73% can be observed in sample S1 for a crack growth of 0.371 mm, while it increases by the negligible value of 1.7% for sample S2 after the crack was propagated by 0.388 mm. A similar trend is also observed in the T-stress.

While the crack length for both samples are about 1.05 mm, ΔK_I for the sample which had experienced an overload is almost one fourth of the sample S1. In addition, ΔK_{II} has increased 74% for sample S1 whereas its changes was negligible for sample S2.

CONCLUSIONS

In this paper, the effect of applying a 40% overload on the behaviour of a crack under cyclic biaxial loading is studied with DIC technique. COD examinations showed the classical sequences of overload including retardation and recovery. A method including fitting the experimental displacement data to analytical solutions based on Williams' series development was also used for studying the biaxial fatigued cracks. This allowed the mixed-mode SIF (K_I and K_{II}) and the T-stress to be estimated on two different

samples, one subjected to an overload event and one without an overload. Results showed that applying 40% overload led to a 27% decrease in ΔK_I after the crack propagated 0.388 mm. ΔK_{II} for the sample which did not experienced overload cycle increased by 73% for a crack growth of 0.371 mm. It was also shown that DIC can effectively be used for studding the structures under biaxial loading.

ACKNOWLEDGEMENTS

Financial support of Junta de Andalucía through Proyectos de Excelencia grant reference TEP-3244; and University of Malaga through Campus de Excelencia Internacional del Mar (CEIMAR) through Líneas Emergentes program and for providing PhD exchange scholarship is greatly acknowledged.

REFERENCES

1. Anderson T.L. (1995) *Fracture Mechanics Fundamentals and Applications*, 2nd ed. CRC Press.
2. ASTM E399-90: *Standard Test Method for Plane-strain Fracture Toughness of Metallic Materials*, *Am. Soc. Test Mater. Annu. B. Stand.* (1991) **3**, 451–85.
3. Suresh, S. (1998) *Fatigue of Materials.* 2nd ed. Cambridge University Press, New York.
4. Ramesh, K., Gupta, S., Kelkar, A.A. (1997) *Eng. Fract. Mech.* **56**, 25–41 and 43–5.
5. Díaz, F.A., Yates, J.R., Patterson, E.A. (2004) *Int. J. Fatigue* **26,** 365–76.
6. Nowell, D., Paynter, R.J.H., De Matos, P.F.P. (2010) *Fatigue Fract. Eng. Mater. Struct.* **33,** 778–90.
7. McNeill, S.R., Peters, W.H., Sutton, M.A. (1987) *Eng. Fract. Mech.* **28,** 101–12.
8. Smith, J., Bassim, M.N., Liu, C.D. (1995) *Eng. Fract. Mech.* **52**, 843–851.
9. Lopez-Crespo, P., Withers, P.J., Yusof, F., Dai, H., Steuwer, A., Kelleher, J.F., Buslaps, T. (2013) Fatigue Fract. *Eng. Mater. Struct.* **36**, 75-84.
10. Sutton, M.A., McNeill, S.R., Helm, J.D., Chao, Y.J. (2000). In: *Photomechanics*, pp. 323–72, Rastogi PK (Ed.), Springer Berlin Heidelberg.
11. Pan, B., Qian, K., Xi,e H., Asundi, A. (2009) *Meas. Sci. Technol.* **20**, 062001 (17pp).
12. Patterson, E.A., Olden, E.J. (2004) *Fatigue Fract. Eng. Mater. Struct.* **27**, 623-635.
13. Sutton, M.A., Orteu, J-J., Schreier, H.W. (2009) *Image Correlation for Shape, Motion and Deformation Measurements*, Springer, New York.
14. Sanford, R.J., Dally, J.W. (1979) *Eng. Fract. Mech.* **11**, 621–33.
15. Yoneyama, S., Ogawa, T., Kobayashi, Y. (2007) *Eng. Fract. Mech.* **74**, 1399–412.
16. López-Crespo, P., Burguete, R.L., Patterson, E.A., Shterenlikht, A., Withers, P.J., Yates, J.R. (2009) *Exp. Mech.* **49**, 551–9.

17. Colombo, C., Vergani, L. (2010) *Eng. Fract. Mech.* **77**, 1644-1655.
18. Zybell, L., Chaves, H., Kuna, M., Mottitschka, T., Pusch, G., Biermann, H. (2012) *Eng. Fract. Mech.* **95**, 45-56.
19. Vasco-Olmo, J.M., Díaz, F.A., Patterson, E.A. (2016) *Int. J. Fatigue* **2** 117-126.
20. Lopez-Crespo, P., Steuwer, A., Buslaps, T., Tai, Y.H., Lopez-Moreno, A., Yates, J.R., et at. (2015) *Int. J. Fatigue*, **71**, 11–6.
21. Lopez-Crespo, P., Mostafavi, M., Steuwer, A., Kelleher, J.F., Buslaps, T., Withers, P.J. (2016) *Fatigue Fract. Eng. Mater. Struct.* doi: 101111/ffe12463.
22. Lopez-Crespo, P., Moreno, B., Lopez-Moreno, A., Zapatero, J. (2015) *Eng. Fract. Mech.* **136**, 115-130.
23. Lopez-Crespo, P., Moreno, B., Lopez-Moreno, A., Zapatero, J. (2014) *Int. J. Fatigue* **71**, 17–25.
24. Lopez-Crespo, P., Garcia-Gonzalez, A., Moreno, B., Lopez-Moreno, A., Zapatero, J. (2015) *Theor. Appl. Fract. Mech.* **80**, 96-103.
25. de Matos, P.F.P., Nowell, D. (2009) *Int. J. Fatigue.* **31**, 1795–804.
26. Yusof, F., Lopez-Crespo, P., Withers, P.J. (2013) *Int. J. Fatigue* **56**, 17–24.
27. Carlson, R., Kardomateas, G., Bates, P. (1991) *Int. J. Fatigue*. **13**, 453–60.
28. Jones, R.E., (1973) *Eng. Frac. Mech.* **5**, 585-604.
29. Williams, M.L. (1957) *J. Appl. Mech.* **24**, 109–14.
30. Zanganeh, M., Lopez-Crespo, P., Tai, Y.H., Yates, J.R. (2013) *Strain* **49**, 102-115.
31. Beretta, S., Rabbolini, S., Bello, A.D. (2015) *Frat. Ed. Integrità Strutt.* **33**, 174–82.
32. Joyce, J.A., Sutton, G.E. (1985) In: *American Society for Testing and Materials*, pp. 225-247, W.H. Cullen, R. W. Landgraf, L. R. Kaizand, and J. H. Underwood (Eds).
33. Lopez-Crespo, P., Shterenlikht, A., Yates, J.R., Patterson, E.A., Withers, P.J. (2009) *Fatigue Fract. Eng. Mater. Struct.* **32**, 418-429.
34. Mokhtarishirazabad, M., Lopez-Crespo, P., Moreno, B., Lopez-Moreno, A., Zanganeh, M. (2016) *Int. J. Fatigue.* doi:10.1016/j.ijfatigue.2016.03.006.
35. Lopez-Crespo, P., Shterenlikht, A., Patterson, E.A., Yates, J.R., Withers, P.J. (2008) *J. Strain. Anal. Eng. Des.* **43**, 769–80.